Talanta 85 (2011) 556–561

Contents lists available at ScienceDirect

Talanta

journal homepage: www.elsevier.com/locate/talanta

Confocal micro-X-ray fluorescence analysis as a new tool for the non-destructive study of the elemental distributions in pharmaceutical tablets

Vincent Mazel[a,*], Ina Reiche[b], Virginies Busignies[a], Philippe Walter[b], Pierre Tchoreloff[a]

[a] Univ Paris-Sud, Laboratoire "Matériaux et santé", EA 401, UFR de Pharmacie, 5 rue Jean Baptiste Clément, 92240 Chatenay Malabry, France
[b] Laboratoire du Centre de Recherche et de Restauration des Musées de France (LC2RMF), UMR 171 CNRS, Palais du Louvre, 14 quai François Mitterrand, 75001 Paris, France

ARTICLE INFO

Article history:
Received 1 February 2011
Received in revised form 7 April 2011
Accepted 11 April 2011
Available online 16 April 2011

Keywords:
Confocal X-ray fluorescence
Chemical imaging
Pharmaceutics
Coating thickness

ABSTRACT

Chemical imaging studies of pharmaceutical tablets are currently an important emerging field in the pharmaceutical industry. Finding the distribution of the different compounds inside the tablet is an important issue for production quality control but also for counterfeit detection.

Most of the currently used techniques are limited to the study of the surface of the compacts, whereas the study of the bulk requires a time-consuming sample preparation. In this paper, we present the use of 3D micro-X-ray fluorescence analysis (3D μXRF) for the non-destructive study of pharmaceutical tablets.

Based on two different examples, it was shown that it was possible to measure the distribution of several inorganic elements (Zn, Fe, Ti, Mn, Cu) from the surface to a depth of several hundred microns under the surface. The X-ray absorption, depending on both matrix composition and energy, is one of the most critical factors of this analytical method while performing depth profiling or mapping. Therefore, an original method to correct the absorption, in order to accurately measure the true elemental distribution, was proposed.

Moreover, by using the presence of titanium dioxide in a pharmaceutical coating, we proved that this technique is also suited to the non-destructive measurement of coating thickness.

1. Introduction

The tablet is nowadays the most widely used pharmaceutical form. It is generally composed of different products including active ingredients and excipients such as diluents, lubricants or gliding agents. These ingredients play a role in the tabletting behavior of the powder but also in the physical properties of the final tablets and finally in the pharmacological efficiency of the product.

All these properties are not only driven by the chemical nature of the products but also by their distribution in the tablet. The composition of the surface layer is, for example, of crucial importance for the *in vivo* release of active ingredients. This distribution is of course a consequence of both the product's physical behavior and the manufacturing process (particularly tabletting). So, being able to study the microscopic structure of the tablets is an important issue in areas such as process monitoring or quality control.

During the last five years, many different types of chemical imaging techniques have been used to study the distribution of compounds at the surface of pharmaceutical tablets. The most widely used are the near-infrared, infrared and Raman spectroscopies [1–13], which are based on vibrational information, but examples of ToF-SIMS imaging [14] for molecular information or micro-X-Ray fluorescence (μXRF) for elemental analysis can also be found [15,16]. Whereas all these techniques are well suited for surface studies, they cannot be used to study distribution inside the tablets without sample preparation, except for the case of confocal micro-Raman spectroscopy. However, studies have shown that, for example, the density of the tablet is not uniform; the tablets are denser near the surface [17] so that, the measurements at the surface may not be representative of the bulk properties. The development of three-dimensional chemical imaging techniques is in these cases of great interest for an improved characterization of pharmaceutical solid forms. In this paper, we attempt to show the potential of such studies using three-dimensional μXRF analyses (3D μXRF).

Three-dimensional or confocal μXRF was first developed using synchrotron sources. The literature gives different examples of the application of the technique for 3D elemental analyses of samples in environmental chemistry, mineralogy or cultural heritage [18–26]. Recently, laboratory set-ups have been developed, avoiding the use of synchrotron radiation sources, which will enable more routine applications of the technique [19,27,28].

X-ray fluorescence is mainly suited to detect and study inorganic constituents or metal-containing organic species. In pharmaceutical tablets, many products containing inorganic elements can be found like titanium dioxide in tablet coating, zinc or magnesium

* Corresponding author. Tel.: +33 01 46 83 54 43; fax: +33 01 46 83 59 63.
E-mail address: vincent.mazel@u-psud.fr (V. Mazel).

0039-9140/$ – see front matter © 2011 Elsevier B.V. All rights reserved.
doi:10.1016/j.talanta.2011.04.027

stearate as lubricants or metal-containing species in vitamin tablets for example. Thus, confocal μXRF can be considered as an interesting technique for pharmaceutical solid forms.

In this paper, two problems were chosen to show the possibilities of this technique to evidence distribution features of components in pharmaceutical tablets. First, laboratory-made tablets containing zinc stearate as a lubricant were used to prove the capability of mapping the distribution of this lubricant by studying the zinc contents inside the tablet. This required, from a methodological point of view, examining the problem of X-ray absorption in the sample and discussing the possible means of absorption correction. Secondly, a commercial coated tablet containing different inorganic ions was studied. It proved possible to map the distribution of the different ions inside the coating but also in the core of the tablet, in a totally non-destructive manner. In addition, this example was also used to highlight another important application of the technique: the non-destructive determination of coating thickness.

2. Material and methods

2.1. Materials

Microcrystalline cellulose, MCC (vivapur 12, 56012100932, JRS, Germany) and Zinc Stearate (Zn-St) were used for laboratory-made tablets.

Tablets of Elevit B9 (Bayer, Germany) are commercially available. A thin foil of titanium (2 μm) was purchased from Goodfellow SARL (Lille, France).

2.2. Tablet formation

Binary mixtures of MCC with 0.5% Zn-St (w/w) were prepared with a Turbula mixer (type T2C, Willy A Bachofen, Switzerland) at 48 rpm for 5 min. Cylindrical tablets were then obtained using an eccentric instrumented Frogerais OA tabletting press. The cylindrical die of 1 cm^3 (section of 1 cm^2 and height of 1 cm) was filled manually. Punches with a diameter of 8 mm were used. During compaction, the compression forces and the punch displacements were recorded using Pecamec software (4.2 version, J2P instrumentation, Vitry sur Seine, France).

2.3. Three-dimensional micro-X-ray fluorescence (3D microXRF)

The confocal arrangement of the μXRF set-up has recently been developed at the C2RMF, Paris. In the Louvre MFX^{3D} set-up, a rhodium tube (iMOXS, IFG, 50 kV, 600 μA) equipped with a full polycapillary lens is used. It provides a spot size of the exciting X-ray beam of about 50 μm at a working distance of about 6 mm. For X-ray detection, an X-Flash SDD detector (Bruker AXS) is mounted. A polycapillary conical collimator (PCCC) with a focal spot size ranging between 35 and 55 μm depending on the X-ray energy is set up in front of this detector. The focal points of the X-ray optics are adjusted so that they form an analytical micro-volume ranging from 35 μm × 35 μm × 35 μm (for high energy X-rays as those emitted by the Zr Kα line) to about 60 μm × 60 μm × 60 μm (for low energy X-rays such as those emitted by the Ca Kα line). The X-ray tube, the detector and the optics are fixed in a specially conceived measuring head. Depth profiles as well as 2D and 3D mapping can be performed by moving the objects through the analytical micro-volume created by the confocal set-up using a motorized xyz stage. Precise movements were achieved thanks to stepping motors with micrometer accuracy. The applicability of such a system, however, is limited by the energy characteristic of the X-ray optics, cutting off at low energies as well as at high energies leaving a usable energy window between 3 and 20 keV. The exact characterisation of the set-up is presented by Reiche et al. (to be published).

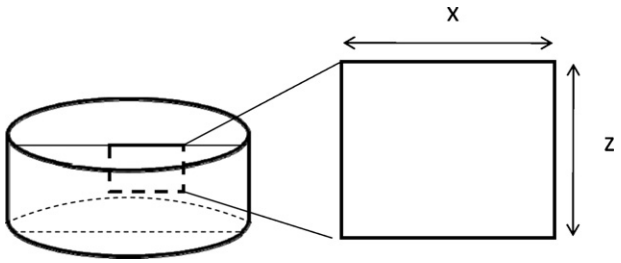

Fig. 1. Schematic representation of the area analyzed in the tablet during 2D *XZ* mapping.

2.4. Scanning electron microscopy

Prior to observation, Elevit B9 tablets were cut with a scalpel blade to obtain a cross-section. The samples were then coated with gold to avoid charge effect.

The apparatus used was a Phillips XP CL 30 series, coupled with an energy dispersive X-ray spectrometer. The accelerated voltage was set to 20 kV and the working distance to 10 mm. Backscattered electrons were used.

3. Results and discussion

3.1. Distribution of Zinc stearate in a laboratory made tablet

The measurements were performed on a tablet obtained with a pressure of 220 MPa. The apparent mean density, calculated according to the tablet dimension and weight, was 1.42 g cm^{-3}.

The experiments were performed in order to obtain 2D *XZ* map, *X* direction being parallel to the surface and *Z* direction being normal to the surface (Fig. 1). This representation leads to a virtual cross-section of the sample and showed the distribution of the lubricant in the bulk. The measurements were performed to a depth of 700 μm and along a line of 1.2 mm parallel to the surface with a step size of 20 μm in both directions (Acquisition time per step: 60 s). The chemical image obtained for Zn is presented in Fig. 2a. It can be clearly seen that the distribution is not homogeneous but consists of small clusters.

Nevertheless, this image does not give an exact representation of the distribution of Zn, because of the partial X-ray absorption in the depth of the sample. X-rays are absorbed by matter according to the Beer-Lambert law that can be written as:

$$I = I_0 e^{-\mu x}$$

where I_0 is the initial intensity of the X-ray beam, I is the intensity after a pathway of a length x in a material with an attenuation coefficient μ. The longer the X-ray path inside the material, the stronger the absorption. The consequence is that the signal detected from the deeper part of the sample appears weaker than it should be. The measured map must therefore be corrected in order to obtain realistic image of the element distribution inside the sample.

In the case of confocal measurements, we know precisely the back and forth trajectories of the X-ray beam inside the sample. In our case, the excitation beam was polychromatic whereas the emission line could be considered as quasi-monochromatic. Therefore, the absorption differed in the two steps. To be able to use a simple Beer-Lambert law, we made two assumptions. Firstly, we assumed that in the energy range where the X-ray production cross-section had significant values, the attenuation coefficient could be considered as constant (or replaced by a mean value). Secondly, we

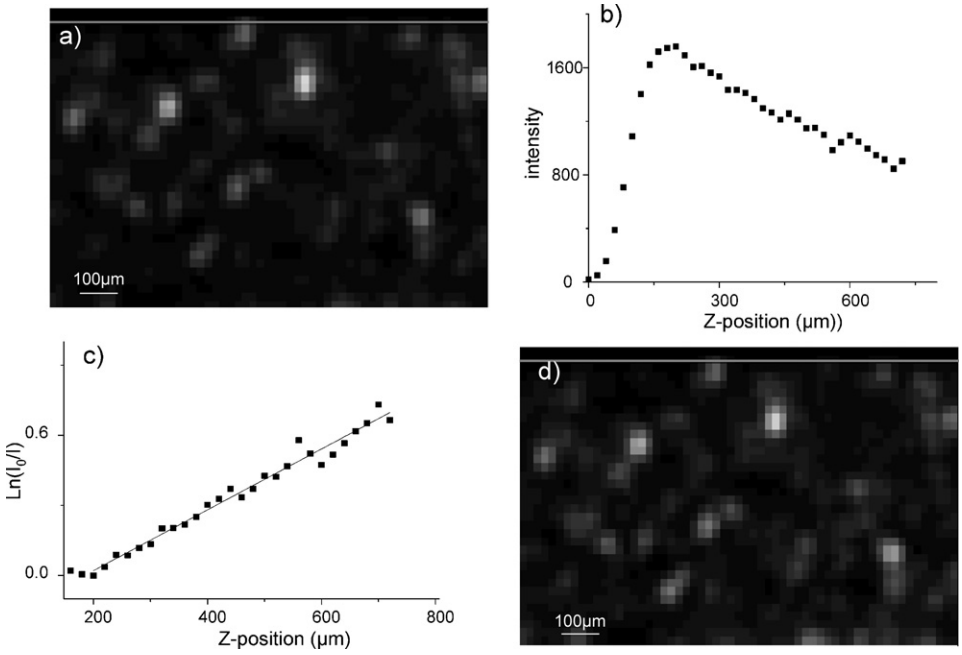

Fig. 2. (a) 2D *XZ* (depth) map of Zn distribution inside a laboratory made tablet (Gray line represent the surface). (b) Intensity depth profile of Rayleigh scattering around 9 keV. (c) Representation of the previous profile using logarithmic function and linear fit according to Beer-Lambert Law. (d) *XZ* distribution of Zinc inside the tablet after absorption correction.

replaced the two values of the attenuation coefficient (the value for each step) by a single mean value, which would be evaluated at an energy level between the absorption edge energy and the emission line energy. These assumptions are also based on the fact that the compact is homogeneous in composition which means the attenuation coefficient is constant in all the material.

But even with this simplification, the attenuation coefficient is difficult to calculate as it depends on both, material density and chemical composition, and the density is known to be inhomogeneous inside the sample. To obtain a value of the attenuation coefficient and perform the correction, an original approach has been chosen based on the evaluation of Rayleigh scattering.

Together with the X-ray fluorescence signal of the element under study, Rayleigh scattering of the incident radiation was detected. The sample was not strongly absorbent and composed of low-Z elements, which gave suitable conditions to use the Rayleigh scattering. As this signal was submitted to the same absorption as the fluorescence signal, it can be used to evaluate the absorption effect. According to the previous discussion, the energy interval to evaluate Rayleigh scattering was chosen between 9 and 9.2 keV (between Kα and Kβ lines) which is in-between the Zn Kα emission line (8.63 keV) and the Kα absorption edge (9.65 keV). The depth profile of the Rayleigh scattering intensity (along *z*-axis) at this energy was plotted by summing values along *x*-axis (parallel to the surface) in order to smooth composition heterogeneity (Fig. 2b). On the graph, an exponential absorption profile can be seen. This curve was used to calculate the attenuation coefficient. Following the Beer-Lambert approach, the logarithm of the ratio between maximum intensity and intensity at particular depth was calculated. This calculation lead to the curve presented in Fig. 2c, which is in accordance with a linear function as expected according to Beer-Lambert law, which validates the approximation made before about the absorption. The slope of the fit function gives the attenuation coefficient. The value obtained is $1.3 \times 10^{-3} \pm 0.1 \times 10^{-3}$ µm^{-1} ($R^2 = 0.976$). This is not directly the attenuation coefficient of the material as it is necessary to take into account the back and forth trajectory in the material and of the fact that the X-ray beam is not normal at the surface. This coefficient can be considered as an apparent attenuation coefficient. Using the model developed by Malzer and Kanngiesser [29], it can be written as:

$$\mu_{app} = \mu \left(\frac{1}{\cos\theta_i} + \frac{1}{\cos\theta_f} \right) \quad (1)$$

where μ_{app} is the apparent attenuation coefficient, μ the real attenuation coefficient and, θ_i and θ_f are respectively the angle of the impinging beam and of the detected beam (both have a value of 45° is the set-up). Using this model lead to a value of $4.6 \times 10^{-4} \pm 0.4$ µm^{-1} for the real attenuation coefficient around 9.1 keV. To verify the consistency of this result, the designed X-ray filter transmission calculator[1] developed by Gullikson and co-workers [30] was used. For a cellulosic material with a density of 1.42 g cm^{-3}, we calculated an attenuation coefficient of 7.1×10^{-4} µm^{-1} at 9.1 keV. The two values were clearly in the same range. Considering that the value of the absorption coefficient was only a mean value due to sample heterogeneity, we believe that both values were close enough to validate our approach for attenuation coefficient determination.

This attenuation coefficient was then used to perform the correction according to the Beer-Lambert law and the result is presented in Fig. 2d. It seems clear, in comparison with the image in Fig. 2a, that the image, after correction, gives a more representative vision of Zn distribution inside the sample. No clear difference can be seen, on the image, between areas near the surface and deeper in the bulk.

The lubricant is present inside the sample as clusters with a roughly homogeneous distribution in the bulk.

3.2. Study of Elevit B9 tablets

3.2.1. Elemental distributions

Elevit B9 is a vitamin and mineral supplement prescribed during pregnancy. It was chosen for its high mineral content and the fact that the tablets were coated. The distribution of several elements

[1] http://henke.lbl.gov/optical_constants/.

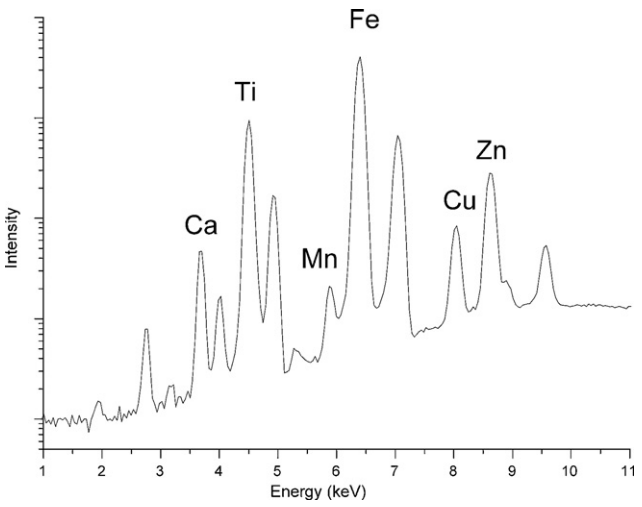

Fig. 3. Global X-ray fluorescence spectra of Elevit B9 tablet.

present in the tablet was investigated using the same set-up as described in the previous case study. Fig. 3 presents the global X-ray fluorescence spectrum, which is the sum of all spectra measured while imaging the sample. The different elements having higher mass than Ca described in the patient leaflet were clearly detected using these measurements (Ti, Mn, Fe, Cu, Zn, Ca). Basically because of the transmission factors of polycapillary optics, the device is not well suited for the detection of lighter elements. The distributions of the elements detected inside the sample are presented in Fig. 4 (step size 20 μm, acquisition time per step 60 s).

The chemical 2D maps clearly reflect the structure of the tablet. The coating and the bulk are easily distinguished due to their different chemical composition and the results are fully consistent with the patient leaflet. Titanium was only found in the coating, and the image shows a quite homogenous distribution. Iron was present both in the coating and in the bulk of the tablet because the coating contains goethite and bulk contains ferrous fumarate. The other elements were part of the bulk. As in the previous example, the results must be taken with caution because of X-Ray absorption. Moreover, as the attenuation coefficient strongly depends on the energy of the X-rays, the correction that should be applied to each image differs. For example, Ca, with a Kα line at 3.69 keV will not be detected as deep as Zn, whose Kα line is at 8.63 keV. Since the sample appeared very heterogeneous, correcting the image using Rayleigh scattering would be difficult and another approach would be necessary.

However, the first conclusion that can be drawn from this analysis is that 3D μXRF is able to detect and map the mineral ingredients beneath the coating level (up to a depth of several hundred microns depending on the element), in a totally non-destructive manner. An additional interesting application of this method is to use the determined element distribution to measure the coating thickness.

3.2.2. Measurement of coating thicknesses

To measure coating thickness, the profile of Ti can be used in the case of Elevit B9 tablets, since this element was only present in the coating. The approach chosen here was based on the model for the confocal volume developed by Malzer and co-workers [29,31]. In this model the sample was assumed to be homogeneous (constant density and attenuation coefficient) and the sensitivity profile of the spectrometer for depth sensitive measurement had a Gaussian profile. The intensity $\varphi(x)$ detected on the probing depth x in a layer can be written as follows:

$$\phi(x) = Ae^{-\mu_{app}(x-d_1)}e^{-(\mu_{app}\sigma)^2/2}\left[\mathrm{erf}\left(\frac{d_2+\mu_{app}\sigma^2-x}{\sqrt{2\sigma}}\right) - \mathrm{erf}\left(\frac{d_1+\mu_{app}\sigma^2-x}{\sqrt{2\sigma}}\right)\right] \quad (2)$$

where μ_{app} is the apparent attenuation coefficient as defined before, σ is the Gaussian width, d_1 and d_2 are the layer boundaries and A is a constant containing both source and layer depending parameters. This model is not strictly applicable in our case as it was developed for a monochromatic excitation. The expression that should be used for polychromatic excitation was developed by Perez et al. [21]. To be able to use Eq. (2) in our case, we needed to make approximations. For the energy dependence of the absorption coefficient, the same approximation as previously used would be used. We assumed that, in the energy range where the production cross-section of the Ka line of Ti had significant values, the attenuation coefficient could be considered as constant. As in the previous case we then replaced the attenuation coefficient by a mean value. We also disregarded the energy dependency of the Gaussian width of the sensitivity profile. For that, we assumed that most of the X-rays that produce fluorescence are, together with the energy of the emission line, in a sufficient narrow range of energy to justify this approximation. Finally, as seen on the image shown in Fig. 4, the coating layer can be considered as homogeneous and we can apply the model to this layer. To determine its thickness, it will be necessary to determine d_1 and d_2 parameters, but also A, μ_{app} and σ.

The Gaussian width is an intrinsic parameter of the spectrometer, which depends on the energy used. It was determined by measuring a thin standard Ti foil of 2 μm thickness with the 3D μXRF set-up. A profile was acquired by moving the probing volume across the foil with a step size of 4 μm (acquisition time per step 25 s). Eq. (2) was then used to fit the obtained depth profile. As we used a foil that can be considered thin enough with respect to the analytical volume, it was possible to disregard the absorption

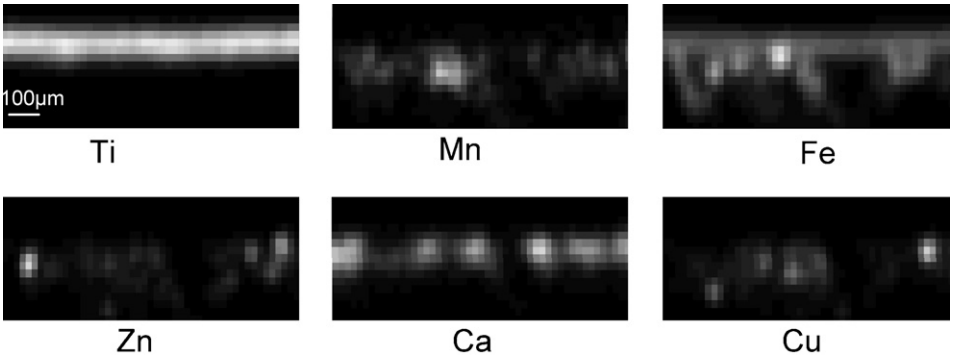

Fig. 4. 2D distribution maps of several element inside Elevit B9 tablet. The surface is at the top of the pictures.

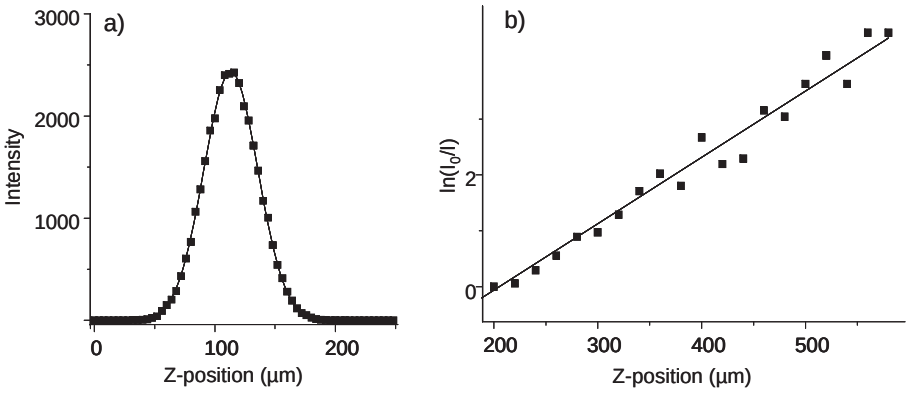

Fig. 5. (a) Intensity profile of a thin Zn foil (2 μm). (b) Beer-Lambert representation and fit of the intensity profile of Rayleigh scattering at 5 keV.

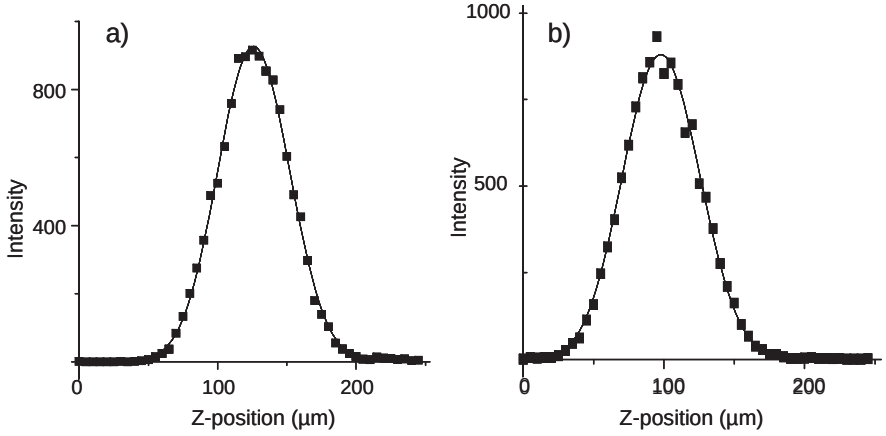

Fig. 6. (a) and (b) Two intensity profiles of titanium in elevit B9 tablet.

in the titanium layer. An example of a Ti depth profile and a fit obtained using Eq. (2) is given in Fig. 5a. The model fits the experimental data perfectly. Five different profiles were measured on the foil. The mean value of the Gaussian width was $\sigma = 22.9 \pm 0.4\ \mu m$. This value was used for the following experiments.

To determine the value of the attenuation coefficient, the approach using Rayleigh scattering was used again. Since the Ti Kα emission line is at 4.51 keV, Rayleigh scattering near 5 keV (from 5.1 keV to 5.3 keV) was chosen. For this purpose, the 2D mapping measurement already presented (Fig. 4) was used and all the spectra along the X direction were summed. The result and the fit are shown on Fig. 5b. The value of the apparent attenuation coefficient was $1.2 \times 10^{-2} \pm 0.1 \times 10^{-2}\ \mu m^{-1}$ ($R^2 = 0.967$). To confirm the physical relevance of this value, we proceeded as in the previous case. Using Eq. (1), this result lead to a real attenuation coefficient of $4.2 \times 10^{-3} \pm 0.4 \times 10^{-3}\ \mu m^{-1}$. The coating was mainly composed of hypromelose and ethylcellulose. If we approximated the sugars as cellulose and assume the layer had a density of $1.5\ g\,cm^{-3}$ (hypromellose has density around $1.7\ g\,cm^{-3}$ and ethylcellulose around $1.2\ g\,cm^{-3}$) an attenuation coefficient of $5 \times 10^{-3}\ \mu m^{-1}$ could be obtained. This value clearly indicates that the apparent attenuation coefficient obtained using Rayleigh scattering is physically relevant.

Finally the previously determined parameters could be used for the fitting function of the Ti profile. Several profiles were measured using a step size of 5 μm (acquisition time per step 40 s). For each profile, three parameters were fitted, A, d_1 and d_2. Two different profiles taken from two different areas of a tablet can be seen in Fig. 6. In each case, the fitting curve accurately describes the measured profile. The obtained values of $d_2 - d_1$, which represents the layer thickness, are $40 \pm 2\ \mu m$ ($R^2 = 0.997$) for the profile of Fig. 6a and $49 \pm 2\ \mu m$ ($R^2 = 0.996$) for the profile of Fig. 6b. To judge the precision of the measurement, a cross-section of the tablet was prepared and observed under scanning electron microscope by means of the backscattered electron image (BSE mode). The electron micrograph is shown in Fig. 7. It appears clearly that coating thickness is not perfectly homogeneous, but measurement performed on the scanning electron micrograph lead to layer thicknesses between 42 and 48 μm. These values are perfectly consistent

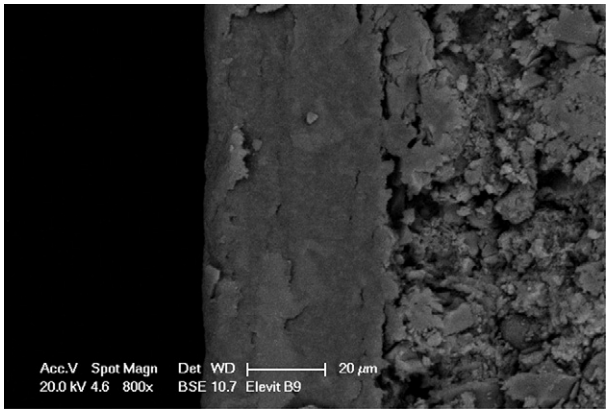

Fig. 7. SEM photograph (BSE) of a cross-section of Elevit B9 tablet, showing the coating level.

with those obtained with the confocal μXRF approach. It can Thus be concluded that the determination of the Gaussian width and the apparent attenuation coefficient were correct. We can also deduce that the approximations were justified. Finally, confocal μXRF appears to be well suited for non-destructive coating thickness measurements.

4. Conclusion

Two cases studies of pharmaceutical tablets highlighted the potential of confocal micro-X-ray fluorescence analysis in a non-destructive method to study representative element distributions inside the tablets. On one hand, it was possible to map the distribution of zinc stearate inside a tablet using an innovative way for the correction of the X-ray absorption in the sample.

On the other hand, by studying the commercial Elevit B9 tablets by means of 3D μXRF, it was possible to map different elements beneath the coating level in depths of several hundred microns depending on the element. Moreover, using the presence of titanium dioxide inside the coating in this tablet, a new original method for the non-invasive measurement of coating thicknesses was proposed. The values obtained by this method are consistent with the SEM observations on the same tablet.

Regarding these results, confocal microX-ray fluorescence can be considered as a new useful tool for the study of pharmaceutical tablets. Whereas obtaining large image takes several hours, depth profiling measurement can be performed in a few minutes. Thanks to the development of a laboratory apparatus, this technique could be used for online quality control but also for counterfeit detection. Fundamental studies of product distribution inside the tablet linked to the manufacturing process are also possible and, in this case, the sensitivity of the measurements and the spatial resolution could be improved by the use of synchrotron radiation.

Acknowledgement

We thank Stella Ghouti for proofreading our document in English.

References

[1] J.M. Amigo, J. Cruz, M. Bautista, S. Maspoch, J. Coello, M. Blanco, TrAC, Trends Anal. Chem. 27 (2008) 696–713.
[2] J.M. Amigo, C. Ravn, Eur. J. Pharm. Sci. 37 (2009) 76–82.
[3] K.L.A. Chan, S.V. Hammond, S.G. Kazarian, Anal. Chem. 75 (2003) 2140–2146.
[4] C.D. Ellison, B.J. Ennis, M.L. Hamad, R.C. Lyon, J. Pharm. Biomed. Anal. 48 (2008) 1–7.
[5] C. Gendrin, Y. Roggo, C. Collet, J. Pharm. Biomed. Anal. 48 (2008) 533–553.
[6] C. Gendrin, Y. Roggo, C. Spiegel, C. Collet, Eur. J. Pharm. Biopharm. 68 (2008) 828–837.
[7] A.A. Gowen, C.P. O'Donnell, P.J. Cullen, S.E.J. Bell, Eur. J. Pharm. Biopharm. 69 (2008) 10–22.
[8] M.B. Lopes, J.-C. Wolff, Anal. Chim. Acta 633 (2009) 149–155.
[9] M.B. Lopes, J.C. Wolff, J.M. Bioucas-Dias, M.A.T. Figueiredo, Anal. Chim. Acta 641 (2009) 46–51.
[10] C. Ravn, E. Skibsted, R. Bro, J. Pharm. Biomed. Anal. 48 (2008) 554–561.
[11] G. Reich, Adv. Drug Deliv. Rev. 57 (2005) 1109–1143.
[12] Y. Roggo, A. Edmond, P. Chalus, M. Ulmschneider, Anal. Chim. Acta 535 (2005) 79–87.
[13] S. Sasic, Anal. Chim. Acta 611 (2008) 73–79.
[14] A.M. Belu, M.C. Davies, J.M. Newton, N. Patel, Anal. Chem. 72 (2000) 5625–5638.
[15] T.C. Miller, G.J. Havrilla, Powder Diffr. 20 (2005) 153–157.
[16] B.M. Patterson, G.J. Havrilla, Appl. Spectrosc. 60 (2006) 471–478.
[17] V. Busignies, B. Leclerc, P. Porion, P. Evesque, G. Couarraze, P. Tchoreloff, Eur. J. Pharm. Biopharm. 64 (2006) 38–50.
[18] B. De Samber, G. Silversmit, R. Evens, K. De Schamphelaere, C. Janssen, B. Masschaele, L. Van Hoorebeke, L. Balcaen, F. Vanhaecke, G. Falkenberg, L. Vincze, Anal. Bioanal. Chem. 390 (2008) 267–271.
[19] B. Kanngiesser, W. Malzer, A.F. Rodriguez, I. Reiche, Spectrochim. Acta, Part B 60 (2005) 41–47.
[20] K. Nakano, K. Tsuji, X-Ray Spectrom. 38 (2009) 446–450.
[21] R.D. Perez, H.J. Sanchez, C.A. Perez, M. Rubio, Radiat. Phys. Chem. 79 (2010) 195–200.
[22] K. Tsuji, T. Yonehara, K. Nakano, Anal. Sci. 24 (2008) 99–103.
[23] L. Vincze, B. Vekemans, F.E. Brenker, G. Falkenberg, K. Rickers, A. Somogyi, M. Kersten, F. Adams, Anal. Chem. 76 (2004) 6786–6791.
[24] X.J. Wei, Y. Lei, T.X. Sun, X.Y. Lin, Q. Xu, D.L. Chen, Y. Zou, Z. Jiang, Y.Y. Huang, X.H. Yu, X.L. Ding, H.J. Xu, X-Ray Spectrom. 37 (2008) 595–598.
[25] B. Kanngiesser, W. Malzer, I. Reiche, Nucl. Instrum. Methods Phys. Res. Sect. B-Beam Interact. Mater. Atoms 211 (2003) 259–264.
[26] K. Janssens, K. Proost, G. Falkenberg, Spectrochim. Acta B 59 (2004) 1637–1645.
[27] I. Mantouvalou, K. Lange, T. Wolff, D. Grotzsch, L. Luhl, M. Haschke, O. Hahn, B. Kanngiesser, J. Anal. At. Spectrom. 25 (2010) 554–561.
[28] K. Nakano, K. Tsuji, J. Anal. At. Spectrom. 25 (2010) 562–569.
[29] W. Malzer, B. Kanngiesser, Spectrochim. Acta, Part B 60 (2005) 1334–1341.
[30] B.L. Henke, E.M. Gullikson, J.C. Davis, At. Data Nucl. Data Tables 55 (1993) 349.
[31] I. Mantouvalou, W. Malzer, I. Schaumann, L. Luhl, R. Dargel, C. Vogt, B. Kanngiesser, Anal. Chem. 80 (2008) 819–826.